Talanta 120 (2014) 230–238

Contents lists available at ScienceDirect

Talanta

journal homepage: www.elsevier.com/locate/talanta

Flow microcapillary plasma mass spectrometry-based investigation of new Al–Cr–Fe complex metallic alloy passivation

N. Ott [a,c,*], A. Beni [b], A. Ulrich [a,1], C. Ludwig [c,d], P. Schmutz [b]

[a] Laboratory for Analytical Chemistry, EMPA – Swiss Federal Laboratories for Materials Science and Technology, 8600 Dübendorf, Switzerland
[b] Laboratory for Joining Technologies and Corrosion, EMPA – Swiss Federal Laboratories for Materials Science and Technology, 8600 Dübendorf, Switzerland
[c] EPFL – École Polytechnique Fédérale de Lausanne, ENAC-IIE, 1015 Lausanne, Switzerland
[d] PSI – Paul Scherrer Institute, ENE-LBK, 5232 Villigen PSI, Switzerland

ARTICLE INFO

Article history:
Received 25 July 2013
Received in revised form
26 November 2013
Accepted 30 November 2013
Available online 6 December 2013

Keywords:
Al–Cr–Fe complex metallic alloys
ICPMS analysis
Flow cell
Microcapillary
Potentiostatic polarization
Passivity

ABSTRACT

Al–Cr–Fe complex metallic alloys are new intermetallic phases with low surface energy, low friction, and high corrosion resistance down to very low pH values (0–2). Flow microcapillary plasma mass spectrometry under potentiostatic control was used to characterize the dynamic aspect of passivation of an Al–Cr–Fe gamma phase in acidic electrolytes, allowing a better insight on the parameters inducing chemical stability at the oxyhydroxide–solution interface. In sulfuric acid pH 0, low element dissolution rates (in the μg cm^{-2} range after 60 min) evidenced the passive state of the Al–Cr–Fe gamma phase with a preferential over-stoichiometric dissolution of Al and Fe cations. Longer air-aging was found to be beneficial for stabilizing the passive film. In chloride-containing electrolytes, ten times higher Al dissolution rates were detected at open-circuit potential (OCP), indicating that the spontaneously formed passive film becomes unstable. However, electrochemical polarization at low passive potentials induces electrical field generated oxide film modification, increasing chemical stability at the oxyhydroxide–solution interface. In the high potential passive region, localized attack is initiated with subsequent active metal dissolution.

1. Introduction

Complex metallic alloys (CMAs) are a new class of crystalline intermetallic phases characterized by a complex crystallographic structure. They are organized in large unit cells, containing hundreds of atoms arranged in highly symmetric clusters, and often considered as stable approximants of quasicrystals [1,2]. Within the CMAs family, Al-based CMAs are promising for future industrial application [2,3]. They are developed to be used as functionalized coatings [4–6] to enhance the aluminum corrosion resistance. Al-based CMAs exhibit a unique combination of surface properties [2,3,7,8], such as low surface energy, low friction coefficient and high stability in a broad pH range [9,10], which depend on their chemical composition rather than on their structural complexity [9,11,12]. Consequently, many of these properties are tightly related to the oxyhydroxide layer, which spontaneously forms on the surface [13]. This nm-thick oxyhydroxide layer, also known as passive layer, continuously undergoes dynamic processes associated with film growth at the metal–oxyhydroxide interface and chemical dissolution at the oxyhydroxide–solution interface. A comprehensive understanding of these processes is therefore necessary to guarantee the material's properties in *operando* conditions for longer service times.

Surface analytical techniques provide useful information about the surface chemical composition, structure, topography and mechanical and electronic properties of passive films [14]. However, they are mainly *ex situ* methods and consequently no mechanistic information about film dynamics can be retrieved. They are usually used in combination with electrochemical methods to determine kinetic data [14]. However, none of these techniques allow full characterization of the dynamic of passivation (including chemical dissolution) at the oxyhydroxide–solution interface.

The electrochemical quartz crystal microbalance (EQCM) proved to be suitable to monitor changes in the passive film induced by electrochemical film growth and chemical dissolution processes at the oxyhydroxide–solution interface with a sub-monolayer mass change sensitivity [15–17]. It could be determined that an increase in the polarization potential leads to an increase of the passive film thickness associated with a significant cation dissolution from the passive film surface. The obtained information remains nevertheless averaged mass changes. Therefore, this method, despite its extremely high sensitivity, only suits for model homogeneous materials.

Over the past years analytical chemistry methods have gained increasing interest in corrosion science. They can provide quantitative information about the element-specific releases even at early corrosion stages, allowing better characterization of the passivation

* Correspondence to: EMPA, Swiss Federal Laboratories for Materials Testing and Research, Laboratory for Analytical Chemistry, Überlandstrasse 129, CH-8600 Dübendorf, Switzerland. Tel.: +41 58 765 4845; fax: +41 58 765 6915.
E-mail addresses: noem.ott@gmail.com (N. Ott), patrik.schmutz@empa.ch (P. Schmutz).
[1] Deceased on March 12th 2013 (A. Ulrich).

0039-9140/$ - see front matter © 2013 Elsevier B.V. All rights reserved.
http://dx.doi.org/10.1016/j.talanta.2013.11.091

dynamics at the oxyhydroxide–solution interface, especially when electrochemical methods are at their current detection limits. In particular, plasma spectroscopy methods, i.e. inductively coupled plasma optical emission spectrometry (ICPOES) and inductively coupled plasma mass spectrometry (ICPMS), present interesting characteristics, such as "fast" multi-element detection, high sensitivity and trace amount detection limits. Nonetheless, these methods are currently mainly used offline, by means of immersion tests, in which the dissolution of a sample in an aqueous environment is followed over time by sampling aliquots of the solution. Analyses are performed afterwards by ICPOES or ICPMS. The whole procedure is consequently time- and sample consuming as well as affected by sampling induced uncertainties.

Hyphenated methods, based on online coupling of an electrochemical flow cell and different downstream analytical techniques [18–26], offer several advantages over conventional immersion tests. Atomic Emission Spectroelectrochemistry (AESEC) [18,19,27–31] or coupling of a microelectrochemical flow cell to an ICPMS [20,21,26] allow determining instantaneous element-specific dissolution rates. Flow microcapillary plasma mass spectrometry on the other hand provides local, time-resolved and element-specific information of corrosion processes under low laminar flow, close to natural convection. It was already successfully applied for corrosion investigations of passive and active systems at open-circuit potential (OCP) [23,32–34]. Coupling of this element-specific technique to electrochemical measurements can be particularly interesting, especially for passive metals, because it provides combined information about transient electrochemical processes at the metal–oxyhydroxide interface and chemical element-specific dissolution at the oxyhydroxide–solution interface.

An important aim of the current study is therefore to present the specifically developed electrochemical microcell for flow microcapillary-based analysis under potentiostatic polarization and to demonstrate its applicability to investigate the dynamic passivation processes of a polycrystalline Al–Cr–Fe gamma phase in acidic electrolytes. This phase exhibits good passivation in extreme pH ranges [9] and is ready to be implemented as a coating in industrial application. Ura et al. [9] showed that the stability of the Al oxyhydroxide layer formed on the Al–Cr–Fe gamma phase relies on the Cr enrichment at the outermost layer. Another relevant aspect for these Al-based alloys is the composition and thickness changes that will be induced in the passive film at long air-aging times [35].

The effect of anodic potentiostatic polarization and air-aging on element-specific dissolution rate were consequently investigated in sulfuric acid at pH 0 by flow microcapillary plasma mass spectrometry analysis under potentiostatic polarization. The strength of this novel experimental method is the simultaneous characterization of both interface reactivity and the identification of discrepancies in the experimental results, which can arise from materials heterogeneities or be inherent to each of the methods used. Most of the published studies only consider one characterization method and, therefore, miss some of the interface processes occurring during passive film formation. The passivation dynamic in a more aggressive environment, i.e. in presence of chlorides, resulting in local destabilization of the oxyhydroxide layer at the oxyhydroxide–solution interface, is also well characterized.

2. Materials and methods

2.1. Samples and solutions

The investigated polycrystalline powder-sintered gamma phases, $Al_{64.2}Cr_{27.2}Fe_{8.1}$ (at. %), were prepared at the "Laboratoire de Science et Génie des Matériaux et de Métallurgie" (Nancy, France) [36]. The polycrystalline gamma phase consists of relatively large grains [9]. Small Al_2O_3 inclusions located at the grain boundaries as well as numerous pull-outs and pores can be observed on the alloy surface due to the production by powder metallurgy. This very fine dispersion of defects may be detrimental for the macroscopic corrosion resistance of the gamma phase [9,10].

The samples were mechanically ground down to 4000 grit silicon carbide paper, polished with diamond paste in ethanol down to 1 μm and then ultrasonically cleaned in ethanol. The final rinsing was performed with isopropanol.

The samples were kept in a desiccator to keep the passive surface in a controlled reproducible low humidity atmosphere. Certain samples were exposed to controlled laboratory conditions ($T=22.2\pm0.2$ °C at 35 ± 2% relative humidity) for a duration between 30 min to 3 h to induce and determine the initial effect of air-aging on the passive layer formation and subsequent stability in acidic media.

Sulfuric acid at pH 0.0 ± 0.3 and hydrochloric acid at pH 2.0 ± 0.3 were used as electrolytes. The solutions were prepared respectively from suprapure sulfuric acid 96% and suprapure hydrochloric acid 30% (Merck, Germany) diluted with MilliQ water (Millipore, Switzerland, 18 MΩ, TOC < 3 ppb).

2.2. Flow microcapillary plasma mass spectrometry

The flow microcapillary plasma mass spectrometer setup (Fig. 1) is based on the coupling of a polypropylene microcapillary (epTips, Eppendorf, Switzerland) to a quadrupole ICPMS Elan 6000 (Perkin Elmer/Sciex, USA) via a FIAS 200 flow injection system (Perkin Elmer/Sciex, USA). As shown in Fig. 2, the flow injection system consists of two incorporated peristaltic pumps and an 8-port switching valve.

A microcapillary (inner diameter of 520 ± 15 μm) is placed on the sample surface and filled with the chosen solution. The total volume within the microcapillary line (microcapillary + tubing) is 450 μl. Continuous circulation of the solution within the microcapillary line is ensured by a peristaltic pump (P2 in Fig. 2) at a flow rate of 600 μl min^{-1}.

The flow injection valve is initially in position 1 (Fig. 2a). In time intervals of 6 min over 120 min, the flow injection valve switches from position 1 to position 2 (injection position), sending the loop content (20 μl) to the ICPMS for element analysis (Fig. 2b). The loop is directly refilled with fresh solution to ensure a constant volume during the whole measurement time. The flow injection valve is then switched back to position 1 (Fig. 2c). During the

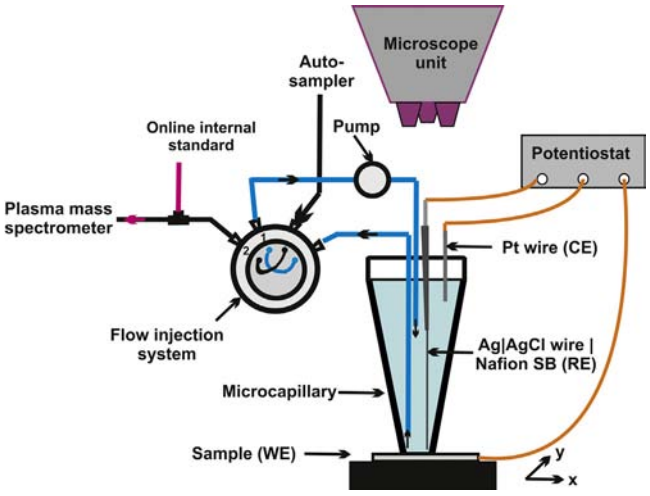

Fig. 1. Flow microcapillary plasma mass spectrometer setup.

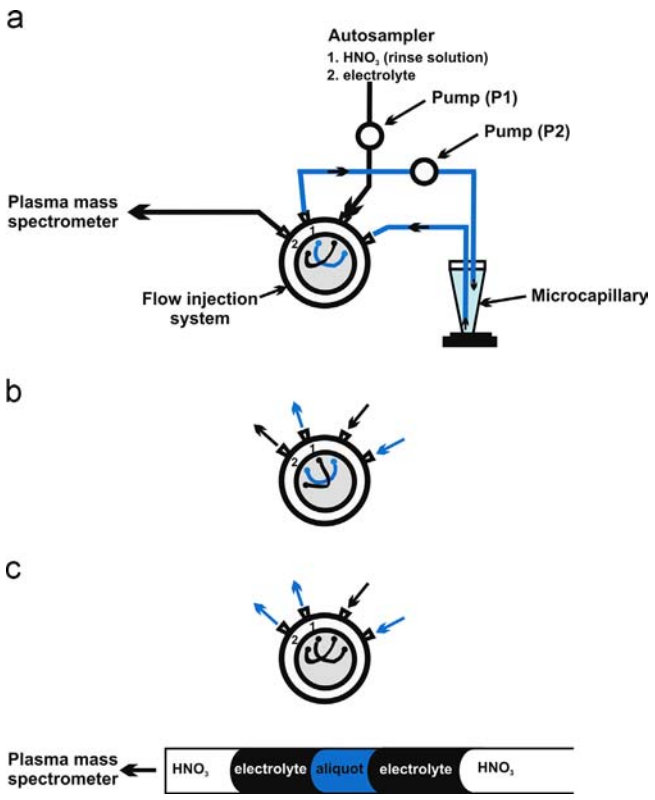

Fig. 2. Flow injection procedure (valve switching) and subsequent flow distribution in the autosampler-ICPMS line.

switching, pump 2 is stopped to prevent volume loss and air bubble formation.

When the aliquot is sent to the ICPMS line, fresh electrolyte is introduced before and after it, as shown in Fig. 2, to limit diffusion phenomena and allow a gain in resolution, since the peak width is drastically reduced. Nitric acid is then continuously sent to the ICPMS for about 3 min to rinse and prevent overload of the ICPMS detector.

In addition, an internal standard solution (20 ppb Ge/Rh) is continuously introduced at an adjusted flow rate of 100 μl min^{-1} through a PEEK Tee (Idex, USA) to the solution stream, which is sent to the ICPMS. It allows controlling the stability of the signal over measurement and compensating the matrix effect due to element dissolution. The internal standard is a stable element, which is not present in the sample itself, but which is chosen in the same mass range and with a similar ionization potential as the measured elements. In this study, germanium (^{74}Ge) was used to correct for non-spectral interferences aluminum signals (^{27}Al) and rhodium (^{103}Rh) to correct for non-spectral interferences chromium and iron signals (^{52}Cr, ^{53}Cr, ^{54}Fe, ^{57}Fe).

A microscope unit was added to the flow microcapillary plasma mass spectrometer setup to allow precise positioning of the microcapillary on the sample surface, which subsequently ensures measurements on the desired investigation area. A xy-scanning stage SCAN 225 × 76 (Märzhäuser Wetzlar, Germany) was therefore combined to a BXFM focusing module (Olympus, Switzerland) equipped with MPLFLN objective lenses (Olympus, Switzerland). The scanning stage is controlled by an in-house developed LabView program. To start with, the distance between the microcapillary and the microscope needs to be newly determined each time. The measurement spot can then be chosen, using the microscope unit. The microcapillary is subsequently accurately fixed at the selected spot with a few μm (± 3 μm) precision. A Dino-Lite Pro (DinoLite Europe, Netherlands) ensures control of the distance between the microcapillary and the sample surface to avoid leakage or unwanted corrosion phenomena, such as crevice corrosion at the microcapillary borders, if too strongly pressed.

2.3. ICPMS analysis

The multi element-specific analysis was performed using an Elan 6000 ICPMS. The ICPMS operating conditions are reported in Table 1. The measured transient signals are normalized through the internal standard intensity. The data are then smoothed by applying a Savitzky Golay filter and peak height is used for the quantitative analysis.

The ICPMS calibration was performed by a flow-injection system using blank solutions and matrix-matched multi-element standard solutions in a concentration range from 2 μg l^{-1} to 100 μg l^{-1}. Five readings per standard were usually run to assess the reproducibility of the obtained data. Limits of detection were determined as three times the standard deviation of the blank solution (3σ method). Only concentrations above the detection limits were taken into account. Typical limits of quantification, calculated as the blank mean value+nine times the standard deviation of the blank solution, are given hereafter: 2.35 ± 0.90 μg l^{-1} for ^{27}Al, 2.47 ± 1.15 μg l^{-1} for ^{52}Cr, 7.62 ± 2.4 μg l^{-1} for ^{53}Cr and 12.93 ± 2.0 μg l^{-1} for ^{57}Fe in H_2SO_4 at pH 0, and respectively, 1.83 ± 0.10 μg l^{-1}, 1.97 ± 0.04 μg l^{-1}, 5.90 ± 0.10 μg l^{-1}, and 8.67 ± 1.5 μg l^{-1} in HCl at pH 2. ^{54}Fe was not considered for data analysis because of the high background created by several interferences on this mass (^{40}Ar^{14}N, ^{54}Cr).

The measured concentrations are corrected with regard to the dilution, which occurs each time an aliquot is sampled out and replaced by fresh solution. The "real" amount of dissolved element at each step can therefore be determined as the sum of the actual measured element concentration and the amount, which was previously sampled, considering the whole microcapillary line volume.

2.4. Electrochemical measurements

Flow microcapillary spectrometry was realized at open-circuit potential (OCP) and under potentiostatic control, using a 200 μm AgIAgCl wire (Science Products, Switzerland) as quasireference electrode (RE) and a 250 μm Pt wire as counter electrode (CE), the sample being the working electrode (WE). The effective surface area exposed to solution at the microcapillary tip is 0.0021 cm^2. The electrodes are directly introduced into the microcapillary. To measure the potential as close as possible to the sample surface,

Table 1
ICPMS operating conditions.

ICPMS instrument	Elan 6000
Operating parameters	
Rf Power (W)	1300
Coolant gas flow-rate (l min^{-1})	15.0
Auxiliary gas flow-rate (l min^{-1})	1.0
Nebulizer gas flow-rate (l min^{-1})	0.95
Ion-sampling parameters	
Sampling and skimmer cones	Nickel
Nebulizer	Micromist 100 μl min^{-1}
Spray chamber	Cinnabar
Data acquisition parameters	
Dwell time (ms)	25
Reading per replicate	300
Number of replicates	5 (standards)/20 (measurements)
Analytes monitored	^{27}Al, ^{52}Cr, ^{53}Cr, ^{54}Fe, ^{57}Fe
Internal standard	^{74}Ge, ^{103}Rh

RE was connected to a Nafion® salt-bridge (SB) introduced in the microcapillary.

The measurements were realized with a modified low-noise battery operated 1002T-NC-3 potentiostat (Jaissle, Germany). Potentiodynamic polarization curves were performed from -0.6 V_{SCE} to 1.0 V_{SCE} at a scanning rate of 1 mV s^{-1}. The potentiostatic measurements were realized at an applied voltage of 0 or 0.5 V versus the quasireference electrode, corresponding respectively to 0.18 V and 0.68 V versus the saturated calomel electrode (SCE), for 120 min with the sample surfaces first kept 5 min at OCP. ICPMS analyses were performed in parallel runs for every 6 min. This can induce some perturbation current transients in the potentiostatic polarization transient curves.

For all data presented in the paper, the potentials were corrected to be expressed versus the SCE true reference electrode. The potential of the Ag|AgCl wire| Nafion® salt-bridge versus the SCE reference electrode was therefore measured before and after each measurement (180 ± 20 mV) and this value was used for correction.

A conventional macroscopic three-electrode cell was used for comparison purposes with a SCE as reference electrode and a Pt grid as counter electrode. The exposed area was in this case 0.20 cm^2.

2.5. Nafion® salt-bridge preparation

Nafion® salt-bridges were preferred to Agar ones under the more acidic conditions of the investigated solutions. The salt-bridges were produced from a mixture of 0.306 ± 0.005 g Nafion® NR50 pellets (Sigma Aldrich, Germany) and 10 ml MilliQ water, conditioned for 20 min at 220 °C in a microwave reactor (Star 1500, MLS GmbH, Germany). The obtained water swelled Nafion® pellets were removed from the aqueous solution. They were then heated in a 2/3 mixture of ethanol and MilliQ water for 120 min at 90 °C. Microloader pipette tips (Eppendorf, Switzerland), used as salt-bridges, were introduced to this gelatinous solution and further heated for 30 min. During baking, the tips are filled by capillary effect. Sulfuric acid was added at the end of the procedure to charge the salt-bridges. The obtained salt-bridges were kept immersed in this solution.

2.6. Qualitative estimation of the passive film thickness

The thickness of the passive film can be determined using the amount of dissolved passive film or the passive film growth at the metal–solution interface with regards to the measured charge transferred. For well passivating, laterally perfect homogeneous materials, both methods should ideally provide similar results but in reality, discrepancies in the determined equivalent thickness can be expected as soon as lateral heterogeneities with different chemical stability are present on the material surface.

The passive film formed on the Al–Cr–Fe gamma phase is assimilated to AlOOH boehmite, based on the XPS analysis reported in [9]. The film density ρ_{film} can be expressed as follows (1):

$$\rho_{film} = c_{Al,film}\, M_{Al} \quad (1)$$

in which $c_{Al,\ film}$ is the Al concentration in AlOOH bohemite (0.0509 mol cm^{-3}) and M_{Al} is the molar mass of Al (27 g mol^{-1}).

The thickness of dissolved passive film ($-\Delta d$) can be estimated using Eq. (2):

$$-\Delta d = \Delta m/(S\, r_x\, \rho_{film}) \quad (2)$$

In this equation, Δm represents the dissolved mass during the measurement, S the effective area, ρ_{film} the film density (1.37 g cm^{-3}) and r_x a rugositiy factor defined by $r_x = A_{real}/A_{geom}$, where A_{real} is the real surface area and A_{geom} the geometrical surface area [15]. The rugosity factor was taken equal to 1 in this study. The dissolved mass, Δm, can be quantitatively determined using ICPMS analysis results, based on chemical dissolution reactions. The equivalent dissolved passive film thickness is expressed as $-\Delta d$ to emphasize the aspect of dissolution.

On the other hand, electrochemical measurements allow estimating the thickness of the formed passive film by considering the cumulated charge transferred during the potentiostatic polarization current transient. From the mass–charge balance, Eq. (3) can be deduced.

$$\Delta d = Q/(n\, Fr_x\, \rho_{film}) \quad (3)$$

In which Q is the integrated charge transferred during the polarization time, n is the number of electrons, F is the Faraday constant, ρ_{film} is the film density (1.37 g cm^{-3}) and r_x is the rugosity factor taken equal to 1.

3. Results

3.1. Nafion® salt-bridge and electrode stability in acidic electrolytes

The potential stability of the quasireference electrode, Ag|AgCl wire and of the Ag|AgCl wire| Nafion® salt-bridge used in sulfuric acid pH 0 media was assessed over 12 h versus a saturated calomel electrode. As shown in Fig. 3, the potential of the Ag|AgCl wire is relatively stable over 12 h (drift within 10 mV). Using a Nafion® salt-bridge, a large drift was observed in the first 120 min in the range of 35–40 mV. The potential stabilized after 120 min. The salt-bridges were therefore kept at least 120 min in H_2SO_4 pH 0 prior to the measurement.

The potential of the Ag|AgCl wire| Nafion® salt-bridge was additionally measured versus a SCE reference electrode before and after the measurements to estimate the drift. The potential drift was within 10 mV over 120 min, which illustrates that excellent stability was maintained over the measurement time.

3.2. Comparative electrochemical potentiodynamic polarization curves

To examine if the electrochemical response of the gamma phase is changed by the use of the flow microcapilary-based setup (Ag|AgCl wire, flow hydrodynamic conditions) and in particular to determine the influence of the salt-bridge on the measurement, comparative potentiodynamic polarization curves were realized with a conventional macroscopic electrochemical cell and the flow microcapillary-based setup under static and hydrodynamic conditions. As shown in Fig. 4, there is no significant difference between the polarization curves recorded using a conventional macroscopic

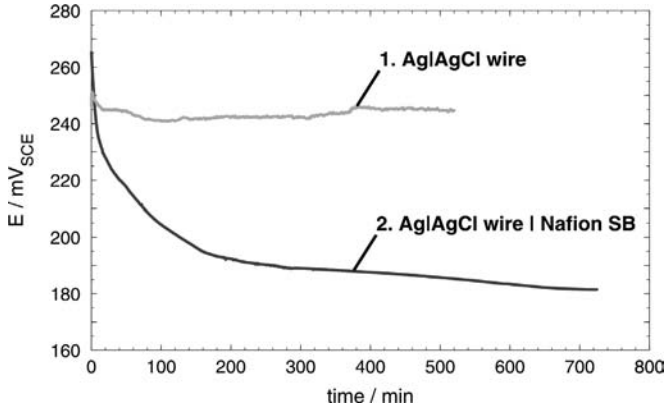

Fig. 3. Electrode potential evolution over 12 h in H_2SO_4 pH 0. 1: Ag|AgCl wire and 2: Ag|AgCl wire|Nafion SB.

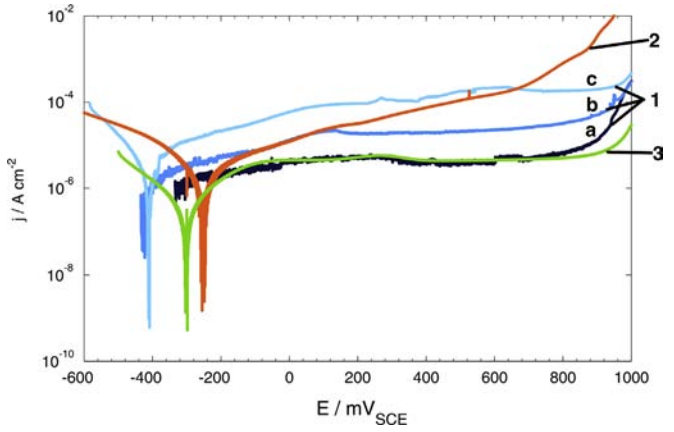

Fig. 4. Polarization curve on Al–Cr–Fe gamma phase in H_2SO_4 pH 0. 1: flow microcapillary-based setup under static conditions after air-aging a. for 30 min b. for 1 h c. for 2 h; 2: flow microcapillary-based setup under hydrodynamic conditions; 3: conventional electrochemical cell.

electrochemical cell (curve #3) and the flow microcapillary-based setup (curves #1 and #2). As already reported in [9,10], gamma phase exhibits passivation in H_2SO_4 solution at pH 0 up to around 900 mV_{SCE} when the Cr oxyhydroxide containing passive film is further oxidized to chromate species. Chromium transpassive dissolution then occurs. These electrochemical polarization measurements show that the Nafion® salt-bridge does not affect the measurement of the electrochemical response of the studied samples.

Three polarization curves (#1 in Fig. 4) were performed on the same sample surface under static conditions but after different exposure time, namely 30 min (#1a), 1 h (#1b) and 2 h (#1c), in controlled laboratory air conditions. Under potentiodynamic polarization, longer air-aging time leads to higher stationary passive current density (curve #1c in Fig. 4), suggesting the presence of a different initial passive oxyhydroxide structure, which is more difficult to stabilize electrochemically.

Under hydrodynamic conditions, the Al–Cr–Fe gamma phase does not exhibit a typical passivation behavior with a current plateau. The potentiodynamic polarization curve (#2 in Fig. 4) shows small but steady current density increases in the passive domain. This suggests that the hydrodynamic conditions in the microcapillary nonetheless slightly change the passivation dynamic.

Nevertheless, these comparative measurements demonstrated the applicability of flow microcapillary-based electrochemical characterization to study the dynamic passivation response (including chemical dissolution) of an Al–Cr–Fe gamma phase in acidic electrolytes. The analytical setup then offers the advantage of local, time-resolved and element-specific investigations under potentiostatic control, which allows simultaneous characterization of both interfaces. The following sections will investigate the chemical dissolution mechanism inducing instability in the passive film at the oxyhydroxide–solution interface in more detail as well as the dynamics of oxide film formation/dissolution at OCP that cannot be assessed by electrochemical methods.

3.3. *Influence of anodic polarization on the element-specific dissolution of Al–Cr–Fe gamma phase*

To get a better insight into the passivation mechanisms of the gamma phase and in particular on the processes at the oxyhydroxide–solution interface, flow microcapillary plasma mass spectroscopy analysis was comparatively performed at OCP, 0.18 V and 0.68 V (versus SCE) in H_2SO_4 at pH 0 on samples aged for 30 min under controlled laboratory air conditions. The two polarization potentials were chosen in the passive region.

As shown in Fig. 5, Cr passive dissolution is extremely low. Polarizing the sample at 0.18 V_{SCE} or 0.68 V_{SCE} slightly increased the Cr dissolution rates in comparison to the one at OCP but they nevertheless remain very small ($< 1.2\ \mu g\ cm^{-2}$ after 120 min). At OCP, Al dissolution is relatively small as well ($10\ \mu g\ cm^{-2}$ after 120 min) but clearly over-stoichiometric compared to Cr with an Al to Cr ratio respectively equal to 200 compared to 2.3 of the alloy composition. Polarizing the gamma surface at 0.18 V_{SCE} leads to no change in Al release. However, increasing the polarization potential to 0.68 V_{SCE} leads to significantly higher Al dissolved amount (about $30\ \mu g\ cm^{-2}$ after 120 min). On the contrary, the polarization of

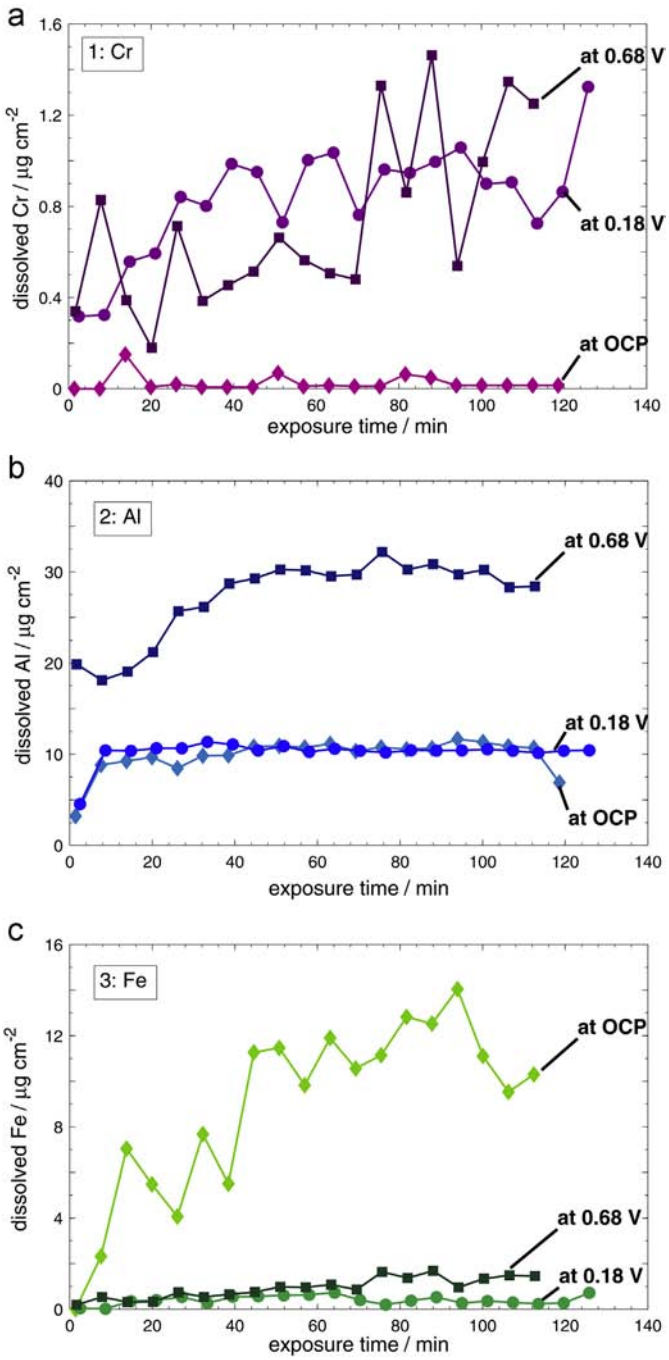

Fig. 5. Dissolved Al–Fe–Cr gamma phase (air-aged for 30 min) in H_2SO_4 pH 0 at OCP and under polarization at 0.18 V_{SCE} or 0.68 V_{SCE}. 1: Cr dissolution rates; 2: Al dissolution rates; 3: Fe dissolution rates.

gamma at 0.18 V_{SCE} or 0.68 V_{SCE} slows down Fe release compared to the one observed at OCP.

The overall element dissolution rate is relatively low. This corresponds to a slow dynamic passive film growth and dissolution. Since neither Al nor Fe is stable as a pure element in this acidic pH [37], chromium is therefore essential to ensure the passive film stability. It helps stabilizing the Al cations within the passive film, as evidenced by the low Al release over 120 min, possibly forming a mixed oxyhydroxide compound. The high dissolved amount of Fe cations detected – with a constant rate over the measurement time – suggests that Fe migration through the passive film to the oxyhydroxide–solution interface occurs. Anodic polarization at 0.18 V_{SCE} or 0.68 V_{SCE} allows slowing down Fe dissolution. Upon polarization at the considered potentials, Fe^{2+}/Fe^{3+} oxidation can take place, leading to the formation of more stable Fe containing mixed oxyhydroxide. But as evidenced by the higher Al dissolution rate, in the high potential passive region, the chemical stability of the passive film at the oxyhydroxide–solution interface is again lowered.

These changes in the passive film stability associated to polarization at high anodic potential can also be observed on the potentiostatic polarization transient curves, shown in Fig. 6. The typical initial sharp current peak resulting from the charge transfer (and capacitive charge of the double layer) is not observed under hydrodynamic conditions, as reported in Fig. 6. However in the steady-state region, the current under static (#1b) or hydrodynamic (#1a) conditions reached the same value, determined by the dissolution of the unstable oxyhydroxides.

Higher current densities were measured at 0.68 V_{SCE} (#2 in Fig. 6) compared to 0.18 V_{SCE} due to the transfer of larger amount of cations and a lower chemical stability of the passive film formed at 0.68 V_{SCE}.

The dynamic passivation mechanism is related to the fact that the cation dissolution occurring at the oxyhydroxide–solution interface (② in Fig. 7) is compensated by additional film growth at the metal–oxyhydroxide interface (① in Fig. 7). The thickness of the passive film can therefore be estimated using Eqs. (2) or (3), which provide respectively the thickness of the dissolved and the formed passive film. For very well passivating materials, the thickness of the formed passive film determined through charge transfer should ideally be similar or slightly larger compared to the dissolved thickness determined by ICPMS analysis.

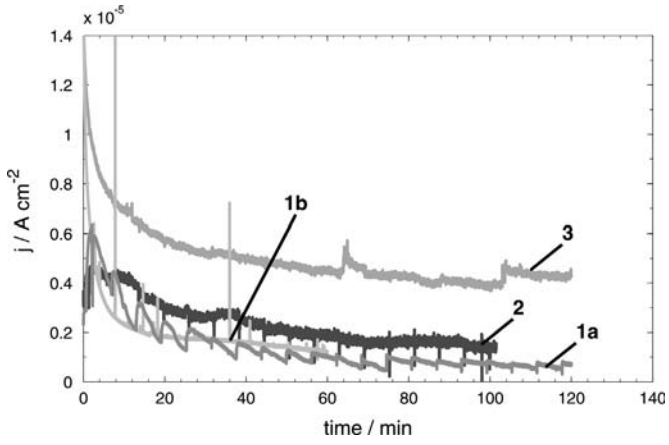

Fig. 6. Potentiostatic polarization curves on Al–Cr–Fe gamma phase (air-aged for 30 min) in H_2SO_4 pH 0 and HCl pH 2, recorded using the flow microcapillary setup. 1: polarization at 0.18 V_{SCE} in H_2SO_4 pH 0 – a. under hydrodynamic condition – b. under static condition; 2: polarization at 0.68 V_{SCE} in H_2SO_4 pH 0 under hydrodynamic condition. 3: polarization at 0.18 V_{SCE} in HCl pH 2 under hydrodynamic condition.

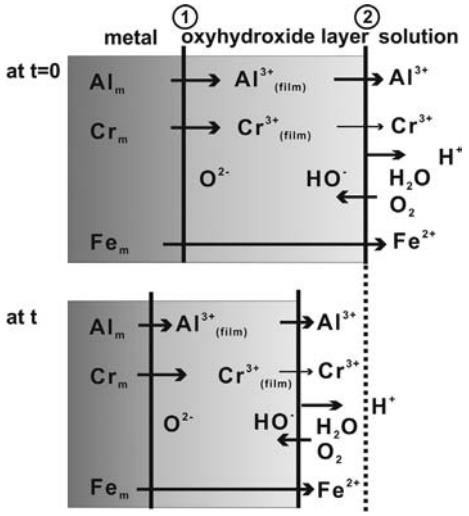

Fig. 7. Schematic showing the dynamic of passive film evolution on an Al–Cr–Fe gamma phase: charge transfer reactions at the metal–oxyhydroxide interface ① and element dissolution at the oxyhydroxide–solution interface ②.

Table 2
Qualitative estimation of equivalent passive film thickness (nm).

Solution	Air-aging	Applied potential	Dissolved passive film thickness (nm)	Formed passive film thickness (nm)
H_2SO_4 pH 0	30 min	OCP	−106	
		0.18 V_{SCE}	−55.6	+8.4
		0.68 V_{SCE}	−153	+6.9
	3 h	OCP	−116	
HCl pH 2	30 min	OCP	−880	
		0.18 V_{SCE}	−147	+24.6

The strength of the present study lies in the ability to determine simultaneously the thickness of the formed and dissolved passive film, which consequently allows proposing a full characterization of the passivation mechanisms. Table 2 reports the qualitative estimation of the equivalent formed and dissolved passive film on the Al–Cr–Fe gamma phase.

The equivalent dissolved passive film thickness after 120 min in H_2SO_4 pH 0 determined by ICPMS measurements represents about 50 nm, corresponding to about two times less than at OCP. Anodic polarization in low potential passive region therefore stabilized the passive film. But when polarizing at a more positive potential, the dynamic between passive growth at the metal–oxyhydroxide interface and dissolution processes at the oxyhydroxide–solution interface is faster. Preferential Fe and Al dissolution can be observed because at a potential close to the chromium transpassive region, stabilization through Cr is no longer sufficient to compensate the instability of the passive film. The equivalent dissolved passive film thickness is estimated at 150 nm after 120 min.

The overall current densities measured during the electrochemical polarization transients however remain in the sub $\mu A\ cm^{-2}$ range, evidencing the passive state of the gamma phase in H_2SO_4 pH 0. The equivalent thickness increase of the passive film formed after 120 min under potentiostatic polarization at 0.18 V_{SCE}, determined through the charge transfer, corresponds to 8.4 nm and to 6.9 nm at 0.68 V_{SCE}. This *a priori* contradicting result in fact evidences the large uncertainty of the current transient signal at the very early stage. The thickness of the passive film formed at 0.68 V_{SCE} is namely expected to be larger compared to the one formed at 0.18 V_{SCE}.

Furthermore it must be pointed out that between the thickness of the formed passive film and the one of the dissolved passive film, there is a factor 10 difference (Table 2). The agreement between the two methods therefore seems very poor. But with a more in-depth analysis of the results, following reasons can be attributed to this difference. On one hand, most of the detected "mass" loss, mainly Al dissolution, occurs at the very early stage of immersion and polarization (ms to s). The ICPMS method presents the advantage of integrating the signal and picking all the Al dissolution. On the contrary, integration of the current transient signal at the very early stage of the transient can be affected by a large uncertainty, especially if the major dissolution should be occurring during a very short time period. In fact, there can be a very short activation period related to the potential step, resulting in an active–passive transition and consequently the current transient might be massively underestimated.

On the other hand, at longer polarization times, ICPMS measurements can also overestimate the dissolved element amount for a very stable passive surface because then any contamination in the microcapillary will become relevant, Al and Fe being critical elements. In case of the Al–Cr–Fe gamma phase investigated here, very fine dispersion of Al_2O_3 inclusions, formed during the powder sintering processes [9] may certainly additionally play a significant role in the discrepancy. Upon exposure to sulfuric acid and even more to hydrochloric acid, dissolution of Al_2O_3 inclusions may occur. The chemical dissolution of these inclusions will be detected by the ICPMS but not by the electrochemical methods, leading to an important overestimation of the dissolved Al amount.

A comparison between both methods is therefore very useful due to the complementarity of the obtained information on heterogeneous materials. Moreover several important conclusions can nevertheless be retrieved from the result discrepancies.

3.4. *Effect of air-aging on the element-specific dissolution of Al–Cr–Fe gamma phase*

Al–Fe–Cr gamma phase samples were kept respectively 30 min, 2 h and 3 h under controlled laboratory air condition (35 % RH, $T=22$ °C) after polishing to estimate the air aging effect on the passive film stabilization and related element-specific dissolution. The open-circuit potential (OCP) evolution, reported in Fig. 8, shows a slight decrease of its value with aging time.

From an element-specific dissolution perspective, Cr remains marginally affected by air-aging with a slightly higher dissolution rate on the air-aged passive layer. Indeed, passive film structure modification might favor Cr cation release. As shown in Fig. 8, Al dissolution rates are much more influenced, its dissolution being slowed down by a factor of 5 after 3 h exposure under controlled laboratory conditions. Unfortunately, the Fe contamination background was too high for the 2 h-aged sample, but the gamma phase sample aged for 3 h under controlled laboratory conditions exhibited a higher Fe dissolution rate than the 30 min air-aged one.

Air-aging seems to promote Al oxyhydroxide film stability. But the structural modification of the passive film during air-aging does not appear to prevent Fe migration to the oxyhydroxide–solution interface and even results in more Cr oxide dissolution. Veys et al. [35] showed that the thickness of the intermediate layer, mainly constituted of Al oxyhydroxide, evolves with aging time and reaches a stable state only after several days.

3.5. *Influence of chlorides on the element-specific dissolution of Al–Cr–Fe gamma phase*

To determine the effect of aggressive chlorides on the oxyhydroxide–solution interface stability and the related element-specific release from the Al–Cr–Fe gamma phase passive surface, measurements were performed at OCP and 0.18 V_{SCE} in an HCl solution at pH 2. As shown in Fig. 9, the gamma phase surface exhibits much

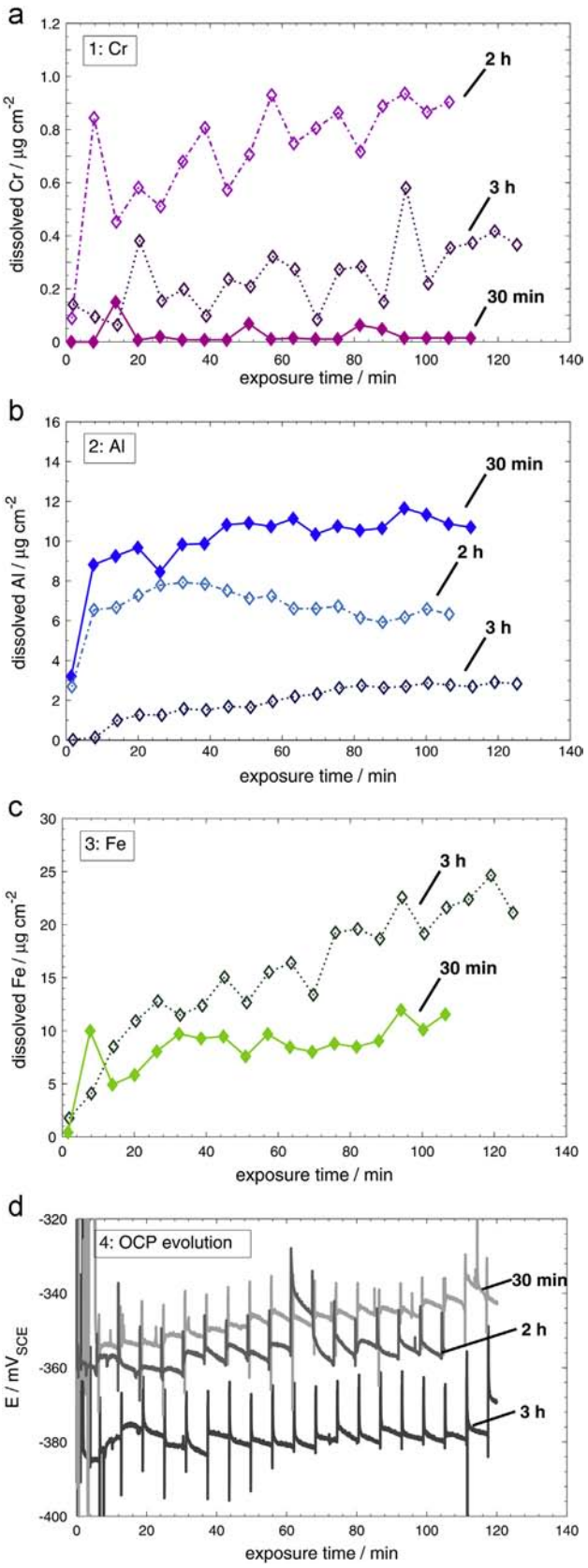

Fig. 8. Effect of air-aging on element-specific dissolution of Al–Cr–Fe gamma phase in H_2SO_4 pH 0 at OCP. 1: Cr dissolution rates; 2: Al dissolution rates; 3: Fe dissolution rates; 4. OCP evolution.

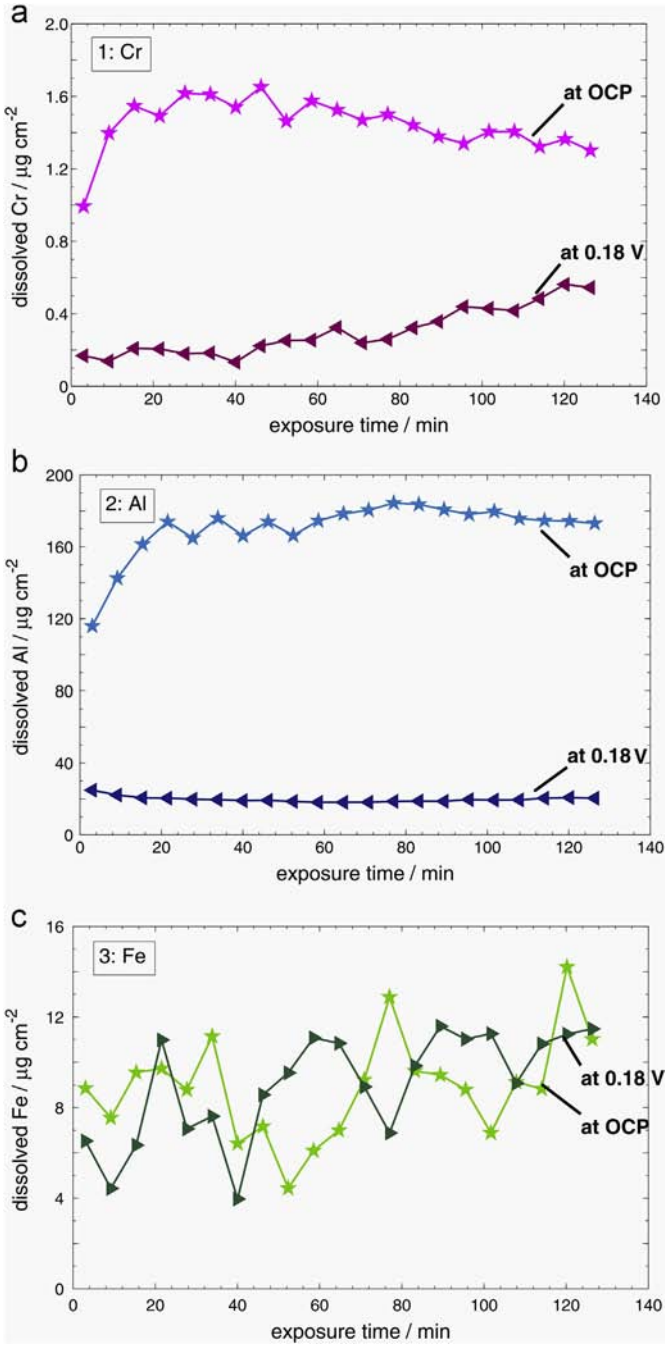

Fig. 9. Element dissolution of Al–Cr–Fe gamma phase (air-aged for 30 min) in HCl pH 2 at OCP and under polarization at 0.18 V_{SCE}. 1: Cr dissolution rates; 2: Al dissolution rates; 3: Fe dissolution rates.

higher Al dissolution in HCl at pH 2 compared to H_2SO_4 at pH 0. At OCP, Al dissolution quickly reached 180 µg cm^{-2} while Cr releases (1.6 µg cm^{-2}) remained low over 120 min even in this aggressive electrolyte. The high Al dissolution rate suggests that Al oxyhydroxide will be destabilized even faster under the action of chloride ions on the surface. Chromium still stabilizes the passive film and consequently protects the gamma phase from "more" severe localized corrosion attack. The dissolution rate of Fe was very over-stoichiometric in sulfuric acid with a Fe to Cr ratio equal to 240 compared to 0.30 in the alloy and remains unchanged in presence of chlorides. But in hydrochloric acid, the Fe/Cr ratio drops to 8, since the Cr dissolution is much higher compared to that in sulfuric acid solutions. These results point out clearly that iron does not participate in the passive film stabilization and consequently simply dissolves at the diffusion rate that can be established through the surface passive oxyhydroxide.

The potentiostatic polarization curve at 0.18 V_{SCE} in HCl pH 2, shown in Fig. 6, presents five times higher current densities compared to the ones measured in H_2SO_4 pH 0. This can again be related to the lower chemical stability of the passive film at the oxyhydroxide–solution interface, resulting in higher cationic dissolution rates (Fig. 9), but the effect seems to be compensated by electrochemical oxide change. What is essential to notice is that the Al dissolution rate during polarization is massively slowed down in comparison to the high dissolution rate observed at OCP. Polarizing the Al–Cr–Fe gamma phase surface at 0.18 V_{SCE} is beneficial, leading to the formation of more stable Al oxyhydroxides by stabilization of the Al^{3+} cations within the passive film. The passive layer formed under low potential polarization in HCl solution at pH 2 is therefore expected to be more stable compared to the spontaneously formed film. Iron dissolution rate remains unaffected by the polarization. It shows once again that Fe dissolution is purely controlled by its migration in the passive film.

The thickness of the dissolved passive film (about 900 nm) at OCP in HCl pH 2 is much higher than in H_2SO_4 pH 0. But even in this aggressive environment, potentiostatic polarization at 0.18 V_{SCE} slowed down the dissolution processes at the oxyhydroxide–solution interface by a factor of 8 (Table 2).

4. Discussion

The present study demonstrates the applicability of flow microcapillary plasma mass spectrometry under potentiostatic control to follow the dynamic passive response, namely the passive film formation and dissolution processes at different interfaces, of a material like the Al–Cr–Fe gamma phase in acidic electrolytes. The high element sensitivity of the ICPMS allows a detailed characterization of the chemical stability and dissolution processes occurring at the oxyhydroxide–solution interface. This time-resolved information cannot be retrieved from conventional electrochemical or XPS measurements but is essential to understand the passivation mechanisms and the stability of the Al–Cr–Fe gamma phase.

Fig. 8 illustrates the dynamics of the passive film evolution on an Al–Cr–Fe gamma phase as function of time. The oxidation of the alloy elements at the metal–oxyhydroxide interface (① in Fig. 7) results in the formation of cations which migrate into the passive film. The dissolution rate at the oxyhydroxide–solution interface (② in Fig. 7) then depends on the solution, namely presence of sulfates or chlorides, and the capacity to form stable corrosion products competing with water induced passivation, etc. The corrosion resistance (uniform and localized) of the Al–Cr–Fe gamma phase is therefore tightly related to this passivation dynamic behavior and cannot be purely assessed with electrochemical methods.

The flow microcapillary plasma mass spectrometer and electrochemical results will be discussed with regards to the XPS analysis realized by Ura et al. [9] on the exact same material.

In sulfuric acid at pH 0, the spontaneous air formed passive film on Al–Cr–Fe gamma phase completely dissolves during the first 120 min, as indicated by the estimated dissolved passive film thickness, but simultaneously reforms. The passive film consequently undergoes structural and composition changes. In H_2SO_4 a thin Al oxyhydroxide layer forms, stabilized by enrichment in Cr at the oxyhydroxide–solution interface, which was not observed on air formed passive films [9,35]. Fe simply dissolves at the migration rate that can be established through the surface oxyhydroxide, as evidenced by its non-detection in the passive oxyhydroxide film. Air-aging of the samples before immersion in sulfuric acid at pH 0 seems to promote passive film stability through the formation of a thicker Al-enriched oxyhydroxide layer at the oxyhydroxide–solution interface. Air-aging probably leads

to structural changes and dehydration of the intermediate layer, which have a beneficial effect on the Al stabilization within the passive film. But it does not limit Fe migration through the passive film.

A qualitative estimation of the dissolved passive film based on the ICPMS analysis showed that anodic polarization in low passive region stabilizes the passive film and therefore slows down the Al–Cr–Fe gamma phase dissolution. However when applying a more anodic potential (0.68 V_{SCE}), instabilities are induced in the passive film. In fact, the more anodic the potential the closer is the Cr transpassive potential. Chromium will therefore not manage to ensure the integrity of the passive film any longer.

The detrimental effect of chlorides is fortunately limited in the case of the Al–Cr–Fe gamma phase due to the stable Cr-enriched oxide layer near the surface. However, due to the preferential formation of aluminum oxy-chloride species at the oxyhydroxide–solution interface [38], Al stabilization within the passive film through chromium is less effective in HCl solutions and results in higher passive Cr dissolution rates at early stages compared to those in sulfuric acid solutions. The formation of these soluble oxy-chlorides at very low pH can favor even faster and more severe dissolution of the microscale Al_2O_3 inclusions present in the powder metallurgical prepared samples. On the other hand, electrochemically anodic treatment of the sample induces the stabilization of Al cations within the passive film again. The corrosion resistance in HCl under potential polarization at 0.18 V_{SCE} is consequently highly increased in comparison to the spontaneously formed passive film at OCP.

Al–Cr–Fe gamma phase exhibits a good passivation in acidic solutions but the surface processes are quite complex. The sample surface can benefit from an electrochemical anodic treatment at low passive potentials, which will stabilize the Al-rich part of the passive layer structure and enhance its corrosion resistance. However, the localized corrosion attacks, especially in chloride-containing solutions, make the choice of the polarization potential critical.

5. Conclusions

Flow microcapillary plasma mass spectrometry under potentiostatic control allows a detailed characterization of the passivation dynamics of the Al–Cr–Fe gamma phase. The high element sensitivity of the ICPMS combined to potentiostatic polarization measurements provide valuable information about the passive film growth at the metal–oxyhydroxide interface and dissolution processes at the oxyhydroxide–solution interface, information which cannot be retrieved purely from electrochemical methods.

The low detected Cr dissolution rates indicate its enrichment within the passive film, and result in very good protective passivation of the Al–Cr–Fe gamma phase.

In sulfuric acid, preferential over-stoechiometric dissolution of Al and Fe cations is observed. Interestingly, Fe can be stabilized by further oxidation in the passive film under polarization although polarization in the high potential passive region leads to increasing Al passive dissolution rates. Air-aging induces structural changes in the passive film, mainly related to dehydration, and therefore Al oxyhydroxides can be stabilized. The passive film is therefore more stable in sulfuric acid but at the same time Fe and Cr dissolution is enhanced.

In presence of chlorides, the passive film spontaneously formed at OCP is very unstable resulting in high initial Al dissolution whereas electrochemical polarization in the low potential passive region leads to stabilization of the passive film again.

Polarization in the low potential passive region consequently allows modifying the passive film structure, slightly thickening the oxide and significantly improving its stability. At higher applied polarization voltage, Cr does not manage to ensure the integrity of the passive film and therefore local passive film breakdown can occur, resulting in lower chemical stability at the oxyhydroxide–solution interface.

Acknowledgments

This work was financially supported by the Swiss National Science Foundation (200020-125121 and 144537). The authors kindly acknowledge Prof. Jean-Marie Dubois and Marie-Cécile de Weerd (Laboratoire de Science et Génie des Matériaux et de Métallurgie, France) for having provided the powder-sintered samples, Rico Muff for the LabView programing, Dr. Magdalena Pawelkiewicz and Dr. Harald Hagendorfer for the fruitful discussions.

References

[1] J.M. Dubois, E. Belin-Ferré, M. Feuerbacher, Introduction to science of complex metallic alloys, in: J.M. Dubois, E. Belin-Ferré (Eds.), Complex Metallic Alloys: Fundamentals and Applications, Wiley-Vch Verlag, Weinheim, 2011.
[2] M.G. Barthes-Labrousse, J.M. Dubois, Philos. Mag. 88 (2008) 2217–2225.
[3] J.M. Dubois, Chem. Soc. Rev. 41 (2012) 6760–6777.
[4] D.J. Sordelet, S.D. Widener, Y. Tang, M.F. Besser, Mater. Sci. Eng.: A 294–296 (2000) 834–837.
[5] J.M. Dubois, Useful Quasicrystals, World Scientific, Singapore, 2005.
[6] J.R. Scully, F. Presuel-Moreno, M. Goldman, R.G. Kelly, N. Tailleart, Corrosion 64 (2008) 210–229.
[7] J.M. Dubois, V. Fournée, P.A. Thiel, E. Belin-Ferré, J. Phys.: Condens. Matter 20 (2008) 314011.
[8] M. Heggen, L. Houben, M. Feuerbacher, Nat. Mater. 9 (2010) 332–336.
[9] E. Ura-Binczyk, N. Homazava, A. Ulrich, R. Hauert, M. Lewandowska, K.J. Kurzydlowski, P. Schmutz, Corros. Sci. 53 (2011) 1825–1837.
[10] A. Beni, N. Ott, E. Ura-Bińczyk, M. Rasinski, B. Bauer, P. Gille, A. Ulrich, P. Schmutz, Electrochim. Acta 56 (2011) 10524–10532.
[11] Y. Massiani, S. Ait Yaazza, J.P. Crousier, J.M. Dubois, J. Non-Cryst. Solids 159 (1993) 92–100.
[12] D. Veys, C. Rapin, X. Li, L. Aranda, V. Fournée, J.M. Dubois, J. Non-Cryst. Solids 347 (2004) 1–10.
[13] M.G. Barthès-Labrousse, A. Beni, P. Schmutz, Surface chemistry of CMAs, in: J. M. Dubois, E. Belin-Ferré (Eds.), Complex Metallic Alloys: Fundamentals and Applications, Wiley-Vch Verlag, Weinheim, 2011.
[14] P. Marcus, F. Mansfeld, Analytical Methods in Corrosion Science and Engineering, Taylor & Francis Group, Boca Raton, 2006.
[15] P. Schmutz, D. Landolt, Electrochim. Acta 45 (1999) 899–911.
[16] P. Schmutz, D. Landolt, Corros. Sci. 41 (1999) 2143–2163.
[17] G.S. Frankel, D. Landolt, Fundamentals, in: M. Stratmann, G.S. Frankel (Eds.), Corrosion and Oxide Films, Wiley-VCH Verlag GmbH & Co, Weinheim, 2003, p. 1.
[18] K. Ogle, S. Weber, J. Electrochem. Soc. 147 (2000) 1770–1780.
[19] D. Hamm, K. Ogle, C.O.A. Olsson, S. Weber, D. Landolt, Corros. Sci. 44 (2002) 1443–1456.
[20] S. Hochstrasser-Kurz, ETH Zürich, Zürich, 2006.
[21] S. Hochstrasser-Kurz, D. Reiss, T. Suter, C. Latkoczy, D. Gunther, S. Virtanen, P.J. Uggowitzer, P. Schmutz, J. Electrochem. Soc. 155 (2008) C415–C426.
[22] N. Homazava, Chemie und Biochemie Fakultät, Universität Bern, Bern, 2009.
[23] N. Homazava, A. Ulrich, U. Krähenbühl, Spectrochim. Acta Part B At. Spectrosc. 63 (2008) 777–783.
[24] N. Homazava, A. Ulrich, M. Trottmann, U. Krähenbühl, J. Anal. At. Spectrom. 22 (2007) 1122–1130.
[25] S.O. Klemm, J.-C. Schauer, B. Schuhmacher, A.W. Hassel, Electrochim. Acta 56 (2011) 4315–4321.
[26] S.O. Klemm, A.A. Topalov, C.A. Laska, K.J.J. Mayrhofer, Electrochem. Commun. 13 (2011) 1533–1535.
[27] K. Ogle, A. Tomandl, N. Meddahi, M. Wolpers, Corros. Sci. 46 (2004) 979–995.
[28] K. Ogle, M. Mokaddem, P. Volovitch, Electrochim. Acta 55 (2010) 913–921.
[29] K. Ogle, J. Baeyens, J. Swiatowska, P. Volovitch, Electrochim. Acta 54 (2009) 5163–5170.
[30] K. Ogle, S. Morel, N. Meddahi, Corros. Sci. 47 (2005) 2034–2052.
[31] P. Volovitch, I. Gazizzullin, F. Ruel, K. Ogle, Corros. Sci. 53 (2011) 1362–1368.
[32] N. Homazava, A. Shkabko, D. Logvinovich, U. Krähenbühl, A. Ulrich, Intermetallics 16 (2008) 1066–1072.
[33] A. Ulrich, N. Ott, A. Tournier-Fillon, N. Homazava, P. Schmutz, Spectrochim. Acta Part B At. Spectrosc. 66 (2011) 536–545.
[34] N. Ott, P. Schmutz, C. Ludwig, A. Ulrich, Corros. Sci. 75 (2013) 201–211.
[35] D. Veys, P. Weisbecker, B. Domenichini, S. Weber, V. Fournée, J.M. Dubois, J. Phys. Condens. Matter 19 (2007) 376207.
[36] V. Demange, F. Machizaud, J.M. Dubois, J.W. Anderegg, P.A. Thiel, D.J. Sordelet, J. Alloys Compd 342 (2002) 24–29.
[37] M. Pourbaix, Atlas of Electrochemical Equilibria in Aqueous Solutions, 2nd ed., NACE International Cebelcor, USA, 1974.
[38] O. Guseva, P. Schmutz, T. Suter, O. von Trzebiatowski, Electrochim. Acta 54 (2009) 4514–4524.